




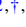


Phases, instabilities and excitations in a two-component lattice model with photon-mediated interactions

Leon Carl ¹, Rodrigo Rosa-Medina ^{1,*}, Sebastian D. Huber ², Tilman Esslinger ¹,
Nishant Dogra ^{3,†} and Tena Dubcek ^{2,†,‡}

¹*Institute for Quantum Electronics, ETH Zürich, 8093 Zürich, Switzerland*

²*Institute for Theoretical Physics, ETH Zürich, 8093 Zürich, Switzerland*

³*Cavendish Laboratory, University of Cambridge, J. J. Thomson Avenue, Cambridge CB3 0HE, United Kingdom*



(Received 20 October 2022; revised 3 March 2023; accepted 14 April 2023; published 11 July 2023)

Engineering long-range interacting spin systems with ultracold atoms offers the possibility to explore exotic magnetically ordered phases in strongly-correlated scenarios. Quantum gases in optical cavities provide a versatile experimental platform to further engineer photon-mediated interactions and access the underlying microscopic processes by probing the cavity field. Here, we study a two-component spin Bose-Hubbard system with cavity-mediated interactions. We provide a comprehensive overview of its phase diagram and transitions in experimentally relevant regimes. The interplay of different energy scales yields a rich phase diagram with superfluid and insulating phases exhibiting density modulation or spin ordering. In particular, the combined effect of contact and global-range interactions gives rise to an antiferromagnetically ordered phase for arbitrarily small spin-dependent light-matter coupling, while global-range and inter-spin contact interactions introduce regions of instability and phase separation in the phase diagram. We further study the low energy excitations above the antiferromagnetic phase. Besides particle-hole branches, it hosts spin-exchange excitations with a tunable energy gap. The studied lattice model can be readily realized in cold-atom experiments with optical cavities.

DOI: [10.1103/PhysRevResearch.5.L032003](https://doi.org/10.1103/PhysRevResearch.5.L032003)

Introduction. Experiments with ultracold atoms in optical lattices have extended the scope of quantum simulations of many-body systems [1,2]. Two key strengths are the high degree of tunability of different energy scales, and the possibility to involve the atomic spin degree of freedom, facilitating the investigation of strongly-correlated phenomena like superfluidity, quantum magnetism, high-temperature superconductivity, and complex out-of-equilibrium dynamics [3,4]. While contact interactions naturally occur in ultracold atomic systems [2,5], long-range interactions have been more elusive. Nonetheless, systems that are traditionally used to study long-range interactions, such as dipolar quantum gases, heteronuclear molecules, and Rydberg atoms, suffer from small long-range interaction strengths, low densities, and short lifetimes, respectively [6–8]. Quantum gases coupled to optical cavities provide an alternative experimental platform to create photon-mediated global-range interactions, whose strength and sign are controlled by external laser fields [9,10]. This has facilitated theoretical [11–19] and experimental [20,21] investigations of lattice supersolid and charge density wave phases in single-component spin systems. The atomic dynamics and many-body excitations can be accessed

nondestructively in real time by the light leaking from the cavity [22]. Recently, the inclusion of an internal atomic spin degree of freedom has become feasible in such systems, leading to the observation of density and spin self-organization [23–25]. Incorporating tunable photon-mediated spin interactions further enriches the accessible phenomenology [26–36]. In combination with optical lattices, this approach will allow the realization of strongly-correlated magnetic phases arising due to the interplay of short- and global-range interactions. Some magnetically ordered phases have been discussed in bosonic [37,38] and fermionic systems [39,40], but a comprehensive theoretical study of the phase diagram and transitions in experimentally accessible regimes is still missing, although it could expedite their successful realization.

Here, we investigate an extended two-component Bose-Hubbard (BH) model with cavity-mediated interactions—the lattice counterpart of the experiment performed in Ref. [23] with a bulk Bose gas. The considered global-range interactions have a “density” and a “spin” contribution, which favor both atomic components to either occupy a common sublattice or two different ones, each breaking independently a lattice \mathbb{Z}_2 -symmetry. Their absolute and relative strengths can be tuned via the intensity and the polarization of an external laser field, respectively. Additionally, the two atomic components have different intra and inter-species contact interactions. We extract the complete phase diagram using a Gutzwiller approach at unity filling, and obtain density-modulated and magnetically-ordered phases, both in the superfluid and insulating regimes. Remarkably, the cooperation between short-range and global-range interactions results in the formation of an antiferromagnetic Mott insulator for arbitrarily small spin-dependent coupling strengths.

*rodrigo@phys.ethz.ch

†These authors contributed equally to this work.

‡dubcekt@ethz.ch

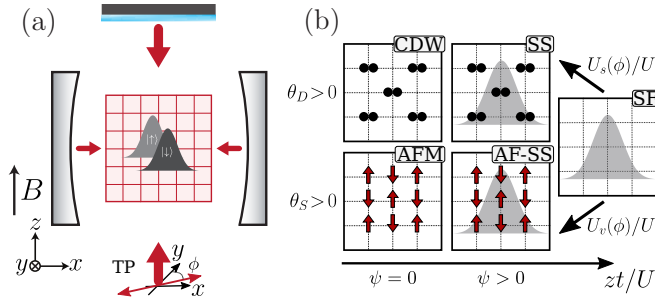


FIG. 1. (a) Schematic representation of a two-component BEC ($|\uparrow\rangle, |\downarrow\rangle$) confined by a 2D optical lattice in an optical cavity. The atoms are illuminated by a transverse pump field (TP) with tunable polarization angle ϕ in the xy plane. (b) Mean-field order parameters and associated phases. The order parameters θ_D, θ_S , and ψ characterize density modulation, spin order and superfluidity, respectively. For $U_{12}/U = 1$, the possible ground states are a superfluid (SF), a charge density wave (CDW), a lattice supersolid (SS), an antiferromagnetic Mott-insulator (AFM), and an antiferromagnetic lattice supersolid (AF-SS). The red arrows and black circles represent the spin states and spin-insensitive density configurations, respectively.

In some regimes, the competing contact-interaction energy scales lead to the separation of the two spin components [41–43]. In addition, global-range interactions can introduce correlated phase-separated states in multicomponent systems [44,45], and induce phase instabilities in systems with only one component [17,46]. To further elucidate the nature of the magnetically ordered phase, we construct an effective Hamiltonian for its low-energy excitations via perturbation theory, and identify spin-exchange branches with a tunable gap.

Description of the system. We consider a balanced spin-mixture of two Bose-Einstein condensates (BECs) coupled to a high-finesse optical cavity. Specifically, we consider ^{87}Rb atoms and a two-dimensional (2D) system extending in the xz plane [Fig. 1(a)], resembling the experiments in Refs. [21,23]. A y -polarized quantized cavity mode is λ periodic, extends along the x axis, and has a resonant frequency ω_c . The two spin components $|\uparrow\rangle = |F=1, m_F=1\rangle$ and $|\downarrow\rangle = |F=1, m_F=-1\rangle$ belong to the total angular momentum $F=1$ manifold, with the quantization axis defined by a magnetic field in the z direction. The mixture is loaded into a 2D $\lambda/2$ -periodic square optical lattice. The lattice arm along z has a frequency ω_p and linear polarization in the xy plane, and fulfills a dual role as a transverse pump field (TP). It is far red-detuned from the atomic and cavity resonance, $\Delta_c = \omega_p - \omega_c < 0$, thus acting dispersively on the atoms. The light scattered from the TP into the cavity couples the atoms' motional and spin degrees of freedom to the cavity mode. The single-particle Hamiltonian reads [47]

$$\hat{H}_{\text{sp}} = \frac{\hat{\mathbf{p}}^2}{2m} + \hat{V}_{\text{lat}} - \left(\Delta_c - U_0 \cos^2 \left(\frac{2\pi}{\lambda} \hat{x} \right) \right) \hat{a}^\dagger \hat{a} + \cos \left(\frac{2\pi}{\lambda} \hat{x} \right) \cos \left(\frac{2\pi}{\lambda} \hat{z} \right) (\eta_s \hat{X} + \eta_v \hat{P} \hat{F}_z) \quad (1)$$

with total momentum $\hat{\mathbf{p}} = (\hat{p}_x + \hat{p}_z)$ and $\hbar = 1$ [23,47]. The first two terms account for the atom moving in the 2D lattice potential $\hat{V}_{\text{lat}} = -V(\cos^2(\frac{2\pi}{\lambda} \hat{x}) + \cos^2(\frac{2\pi}{\lambda} \hat{z}))$.

The operator \hat{a}^\dagger denotes the creation operator associated with the intracavity field. The effective cavity detuning is $\tilde{\Delta}_c = \Delta_c - U_0 \cos^2(\frac{2\pi}{\lambda} \hat{x}) < 0$, with $U_0 < 0$ being the maximal dispersive shift per atom [47]. The last term in Eq. (1) describes a self-consistent interference potential that arises due to light scattering between the TP and the cavity mode [47]. The scalar component of the atom-light interactions couples the atomic motional degrees of freedom to the real quadrature of the cavity field, $\hat{X} = (\hat{a} + \hat{a}^\dagger)/\sqrt{2}$, giving rise to a λ -periodic spin-independent density modulation. The vectorial coupling is mediated by the imaginary quadrature, $\hat{P} = i(\hat{a}^\dagger - \hat{a})/\sqrt{2}$, and gives rise to phase-shifted λ -periodic modulations for the two spin states, since the z component of the atomic spin operator $\hat{\mathbf{F}}$ yields $\hat{F}_z |\uparrow\rangle = +|\uparrow\rangle$ and $\hat{F}_z |\downarrow\rangle = -|\downarrow\rangle$. The associated coupling strengths are $\eta_s = \eta \cos(\phi)$ and $\eta_v = \eta \xi \sin(\phi)$, with $\xi = \frac{\alpha_v}{2\alpha_s}$ given by the atom-cavity coupling rate η and the ratio of the scalar and vectorial polarizabilities [48,49].

We adiabatically eliminate the intracavity field in a tight-binding approximation [14,21,47,50] and obtain a BH Hamiltonian,

$$\hat{H} = \hat{H}_{\text{BH}} + \hat{H}_{\text{Global}}, \quad (2)$$

with

$$\hat{H}_{\text{BH}} = -t \sum_{m, \langle \mathbf{i}, \mathbf{j} \rangle} (\hat{b}_{\mathbf{i}, m}^\dagger \hat{b}_{\mathbf{j}, m} + \text{H.c.}) + \frac{U}{2} \sum_{\mathbf{i}, m} \hat{n}_{\mathbf{i}, m} (\hat{n}_{\mathbf{i}, m} - 1) + U_{12} \sum_{\mathbf{i}} \hat{n}_{\mathbf{i}, \uparrow} \hat{n}_{\mathbf{i}, \downarrow}, \quad (3)$$

and

$$\hat{H}_{\text{Global}} = -\frac{U_s}{K} \hat{\Theta}_D^2 - \frac{U_v}{K} \hat{\Theta}_S^2. \quad (4)$$

The first term, Eq. (3), constitutes a two-component BH model [1,2,41,42,51], comprising tunneling to the z nearest neighbors, with rate $t > 0$ and repulsive intra and interspin contact interactions, $U > 0$ and $U_{12} > 0$. We assume the former to be identical for $|\uparrow\rangle$ and $|\downarrow\rangle$, as is the case for ^{87}Rb in the $F=1$ hyperfine groundstate manifold [52]. The operator $\hat{b}_{\mathbf{i}, m}^\dagger$ denotes the bosonic creation operator, while $\hat{n}_{\mathbf{i}, m} = \hat{b}_{\mathbf{i}, m}^\dagger \hat{b}_{\mathbf{i}, m}$ counts the total number of atoms with spin $m \in \{\uparrow, \downarrow\}$ at site $\mathbf{i} = (i_x, i_z)$. For sufficiently large magnetic fields, both spin-changing collisions and cavity-assisted Raman processes can be neglected [52]. The second term, Eq. (4), consists of spin-independent (“scalar”) and spin-dependent (“vectorial”) global-range interactions that are mediated by the intracavity field. The scalar interactions are associated with the operator $\hat{\Theta}_D^2 = (\sum_{\mathbf{i}} (-1)^{|\mathbf{i}|} \hat{n}_{\mathbf{i}})^2$, where $|\mathbf{i}| = i_x + i_z$ and $\hat{n}_{\mathbf{i}} = \hat{n}_{\mathbf{i}, \uparrow} + \hat{n}_{\mathbf{i}, \downarrow}$. Its expectation value is maximized for a spin-independent spatial density modulation with all atoms occupying only even or odd sites. The expectation value of the operator associated with vectorial interactions, $\hat{\Theta}_S^2 = (\sum_{\mathbf{i}} (-1)^{|\mathbf{i}|} \hat{S}_{z, \mathbf{i}})^2$ with $\hat{S}_{z, \mathbf{i}} = \hat{n}_{\mathbf{i}, \uparrow} - \hat{n}_{\mathbf{i}, \downarrow}$, is maximized for a global antiferromagnetic ordering of the atoms, with all atoms in $|\uparrow\rangle$ occupying even sites and all atoms in $|\downarrow\rangle$ occupying odd sites, or vice versa. The interaction strengths $U_s = U_L \cos^2 \phi$ and $U_v = U_L \xi^2 \sin^2 \phi$ can be tuned with respect to each other via the angle ϕ . The overall interaction strength $U_L > 0$ depends on $\tilde{\Delta}_c$ and the lattice depth V [47]. The total number of sites is denoted by K .

Remarkably, the energy scales of the tunneling, contact and global-range interactions are all independently tunable with respect to each other. The latter increase linearly, both with the number of sites and atoms $U_L \propto K = N$ [47], due to the collective enhancement of photon scattering into the cavity by the number of atoms, provided the cavity mode size does not become a limiting factor [14,21]. The Hamiltonian, Eq. (2), is invariant under a global spin-flip $\hat{b}_{i,\uparrow} \rightarrow \hat{b}_{i,\downarrow}$ and two global rotations $\hat{b}_{i,m} \rightarrow e^{i\phi_m} \hat{b}_{i,m}$ for each $m \in \uparrow, \downarrow$. Furthermore, the scalar and vectorial global-range interactions introduce an additional \mathbb{Z}_2 symmetry associated to the two sublattices defined by even and odd sites. Henceforth, the Hamiltonian has a $\mathcal{U}(1) \times \mathcal{U}(1) \times \mathbb{Z}_2 \times \mathbb{Z}_2$ symmetry.

Gutzwiller ansatz and order parameters. Motivated by the large particle numbers in experimental platforms $N \approx 10^4$ [21,23], we explore the zero-temperature phase diagram by using a Gutzwiller mean-field approach and considering the case of unity filling ($K = N$) [53–55]. We assume a translationally invariant ground state on each of the even (e) and odd (o) sublattices:

$$|\Psi_G\rangle = \prod_{e=0}^{K/2} \prod_{o=0}^{K/2} |\phi_e\rangle |\phi_o\rangle. \quad (5)$$

For each site $i \in \{e, o\}$, the wave function is given by

$$|\phi_i\rangle = \sum_{n=0}^{n_{\max}} \sum_{m=0}^{m_{\max}} a_i(n, m) |n, m\rangle_i, \quad (6)$$

where $|n, m\rangle_i = \frac{(\hat{b}_{i,\uparrow}^\dagger)^n (\hat{b}_{i,\downarrow}^\dagger)^m}{\sqrt{n!} \sqrt{m!}} |0\rangle$ is the local Fock state with $n \leq n_{\max}$ atoms in spin state $|\uparrow\rangle$ and $m \leq m_{\max}$ atoms in state $|\downarrow\rangle$ on a single site. The real coefficients $\mathbf{a}_e \equiv (a_e(n, m))_{n,m}$ and $\mathbf{a}_o \equiv (a_o(n, m))_{n,m}$ are optimized to minimize the effective mean-field energy density

$$\mathcal{E}(\mathbf{a}_e, \mathbf{a}_o) = \frac{\langle \Psi_G | \hat{H} | \Psi_G \rangle}{K/2}. \quad (7)$$

The superfluid order parameter $\psi = \frac{1}{4} \sum_{i,m} \psi_{i,m}$ with $\psi_{i,m} = |\langle \hat{b}_{i,m}^\dagger \rangle|$ ($m \in \{\uparrow, \downarrow\}$) signals the transition from an insulating phase ($\psi = 0$) to a phase-coherent superfluid phase exhibiting off-diagonal long-range order ($\psi > 0$). The density $\theta_D = |\langle \hat{n}_e - \hat{n}_o \rangle|$, and spin $\theta_S = |\langle \hat{S}_{z,e} - \hat{S}_{z,o} \rangle|$ order parameters indicate the degree of global spatial density and spinordering due to global-range interactions [Fig. 1(b)].

Phases for a uniform mixture. We discuss the case of a balanced spin mixture for $U_{12} = U$ at unity filling

$$\rho_m = \frac{N_m}{(K/2)} = \langle \phi_e | \hat{n}_{e,m} | \phi_e \rangle + \langle \phi_o | \hat{n}_{o,m} | \phi_o \rangle = 1 \quad (8)$$

with $m = \uparrow, \downarrow$. The choice of fixed density is motivated by experiments with ultracold atoms, although a qualitatively similar phase diagram arises in a grand canonical ensemble [37,47]. The different order parameters are shown in Fig. 2. The competition of scalar and vectorial global-range interactions gives rise to two qualitatively different scenarios.

For $U_s > U_v$ [Figs. 2(a) and 2(b)], we observe two distinct insulating phases ($\psi = 0$) at low tunneling rates zt/U : For large U_L , a spin-degenerate charge density wave (CDW), with

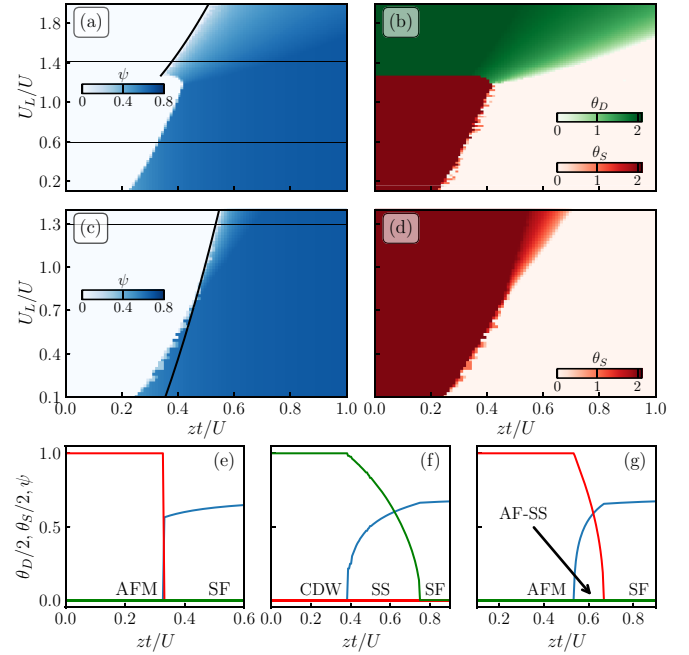


FIG. 2. Mean-field phase diagrams for a balanced-spin mixture at unity filling for $U_s/U_v \approx 4.64$ (a), (b) and $U_s/U_v \approx 0.33$ (c), (d). (a), (c) Dependence of superfluid order parameter ψ . The solid lines are perturbative estimations for the transition. (b), (d) Dependence of density and antiferromagnetic order parameters θ_D and θ_S . (e)–(g) Cuts along the phase diagrams for $U_s/U_v \approx 4.64$ at constant $U_L/U = 0.59$ and $U_L/U = 1.41$ (e), (f) and for $U_s/U_v \approx 0.33$ at $U_L/U = 1.3$ (g), indicated by horizontal lines in (a), (c).

$\theta_D > 0$ and $\theta_S = 0$; and for small U_L , an antiferromagnetic Mott insulator (AFM), with $\theta_S > 0$ and $\theta_D = 0$. Remarkably, the system favors an AFM for arbitrarily small U_L : the contact interaction hinders the formation of a CDW and overcomes the kinetic energy cost to form a unity filling Mott insulator (MI). There, the AFM configuration is favored among all possible MIs by the vectorial interactions. The discontinuity in the order parameters θ_D and θ_S when modifying U_L/U at fixed zt/U signals a first order AFM-CDW phase transition, occurring at $U_L/U \approx 1.27$ [47]. As tunneling increases, the system becomes superfluid ($\psi > 0$) and we observe a first-order AFM-SF phase transition at small U_L/U , signaled by a discontinuous jump in the order parameters [Fig. 2(e)]. For larger global-range interactions, the superfluid phase exhibits density ordering (θ_D), which we denote as a lattice supersolid (SS). While in the insulating regime, the AFM phase is stabilized by contact interactions for $U_s < U/2 + U_v$ [47]; In the superfluid regime a SS phase is favored for a small region around $U_L/U = 1.22$, giving rise to a first-order AFM-SS phase transition. For even larger U_L/U a second-order CDW-SS occurs, see Fig. 2(f).

In the regime $U_v > U_s$ [Figs. 2(c) and 2(d)], the system exhibits solely spin ordered phases ($\theta_S > 0$ and $\theta_D = 0$), as the vectorial global-range and the contact interactions dominate over the scalar interactions. For small U_L , we identify a first-order AFM-SF phase transition, signaled by a discontinuous jump of ψ and θ_S [Fig. 2(e)]. We observe an increase of the von Neuman entropy when transitioning to the super-

fluid phase [47], indicating local entanglement between the two spin components. For larger U_L , we observe a second-order transition from AFM to a spin-ordered superfluid phase, which we denote as an antiferromagnetic lattice supersolid phase (AF-SS) [Fig. 2(g)]. The second-order phase transitions from AFM to AF-SS and CDW to SS are supported by perturbative estimations, cf. black lines in Figs. 2(a) and 2(c) [47,56]. The qualitative behavior of these transitions also agrees with exact diagonalization calculations, which are however limited to small system sizes [47].

As the global-range interactions couple every pair of lattice sites, they are captured well by our mean-field Gutzwiller ansatz [57]. However, we expect the method to progressively lose validity as the tunneling is increased, since the local-basis truncation ($n_{\max} = m_{\max} = 3$) disregards large local occupations that are present deep in the superfluid regime [55]. This is reflected by the saturation of ψ in Figs. 2(e)–2(g).

Phases for different U_{12}/U . Besides homogeneous stable phases, the system can host phase separation (PS) and phase instability (PI) in certain regions of the phase diagram. On the one hand, for large interspin interactions U_{12}/U , it becomes favorable for the two spin species to separate in space [37,41–45,58,59]. This is reflected in a lower energy of the PS state in comparison to its spatially homogeneous counterpart. To allow for a PS state, the system is divided into halves (A, B): one with higher spin-up density ($\rho_{\uparrow}^A > \rho_{\downarrow}^A$) and one with higher spin-down density ($\rho_{\downarrow}^B > \rho_{\uparrow}^B$), while imposing a density conservation constraint in each half, $\rho \equiv \rho_{\uparrow}^{A,B} + \rho_{\downarrow}^{A,B} = 2$, to ensure unity filling. We further assume either $\langle \hat{\rho}_D \rangle = 0$ or $\langle \hat{\rho}_S \rangle = 0$. On the other hand, phases obtained at fixed density may become unstable when densities are allowed to fluctuate. Bose-Hubbard models with concurring long-range [46] or global-range interactions [17] are known to feature phase instabilities. Such instabilities are signaled by a negative compressibility, $\partial_{\rho} \mu < 0$ [46], where $\mu(\rho) = \partial_{\rho} \mathcal{E}(\rho)$ is the chemical potential as a function of the density ρ . We calculate the derivative numerically by using the energy densities $\mathcal{E}(\rho)$ extracted from the variational ansatz in Eq. (7) allowing for density variations [47].

We now discuss the phase diagrams for different inter to intraspin interaction ratios U_{12}/U , and scalar to vectorial global-range interaction ratios U_s/U_v . Without the constraint of spatially homogeneous solutions, the mixed CDW state $|\phi_e, \phi_o\rangle = |\uparrow\downarrow, 0\rangle$, the entangled state $|\phi_e, \phi_o\rangle = |\uparrow\uparrow, 0\rangle + |\downarrow\downarrow, 0\rangle$, and the fully PS configuration with $\rho_{\uparrow}^A = \rho_{\downarrow}^B = 2$ become degenerate at $U_{12}/U = 1$ [Fig. 3(b)].

The phase diagrams for $U_{12}/U < 1$ are qualitatively similar to the $U_{12}/U = 1$ uniform mixture for all U_s/U_v ratios. For dominating scalar interactions, we observe an enlarged CDW region toward both AFM and SS phases as U_{12}/U drops, explained by the smaller local cost of double site occupation. We additionally find a region of PI in the SS phase for $U_{12} \leq U$. Our observations of PI are qualitatively different from the results for spinless systems [17,46], which predict stable SS phases at integer filling in 2D systems. For dominating vectorial interactions, we find extended regions of PI in the AF-SS phase.

With stronger interspin interactions, $U_{12}/U > 1$, several fully PS phases arise. For dominating scalar interactions, we observe a fully PS CDW and PS SS. We find a fully PS SF for

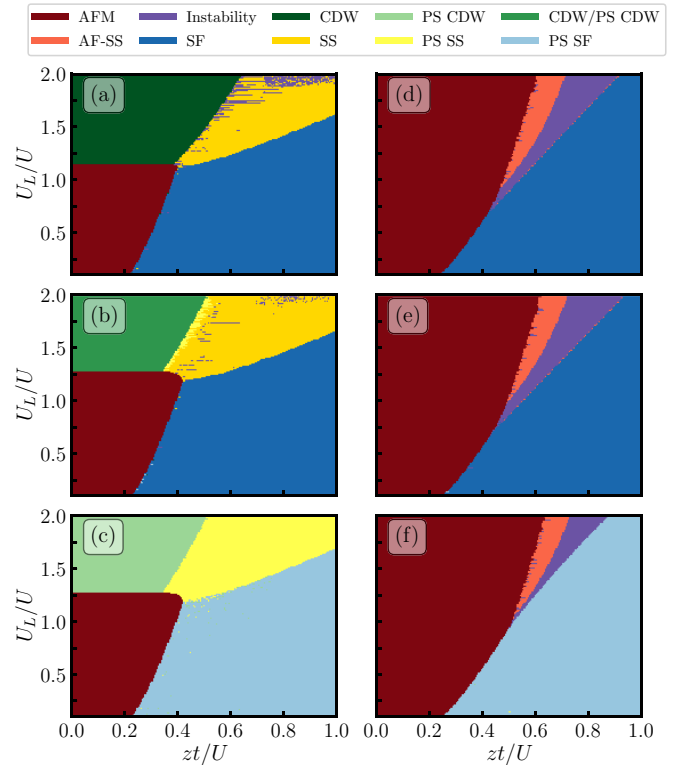


FIG. 3. Mean-field phase diagrams for $U_{12}/U = 0.9$ (a), (d), 1 (b), (e), and 1.1 (c), (f) at $U_s/U_v \approx 4.64$ (a)–(c) and $U_s/U_v \approx 0.33$ (d)–(f). A total average density of $\rho = 2$ is considered.

all U_s/U_v ratios. We also observe a shrinkage of the AF-SS region as U_{12}/U grows, explained by the increasing local cost of double site occupation with atoms of opposite spin. In contrast, the boundaries between insulating regions (PS CDW, AFM) and the PS noninsulating state (PS SS, PS SF) do not change with U_{12}/U , as the energies of the PS phases and the AFM phase do not depend on U_{12} .

We note here two limitations of our simulations. First, the identification of the different phases relies on numerical minimization [47] in a high-dimensional landscape. This can lead to spurious solutions, such as the scattered instability points in Figs. 3(a) and 3(b) and the irregular phase boundaries in Figs. 2 and 3. Second, there is a small region of fully PS SS for $U_{12} = U$ and $U_s/U_v > 1$, cf. Fig. 3(b). This is due to the relatively small Hilbert space ($n_{\max} = m_{\max} = 3$) used for the simulations. We expect that a larger Hilbert space would lead to degenerate SS and PS SS solutions. Additional information on the properties of the various phases, the nature of phase transitions, and the identification of phase separation and phase instability is presented in [47]. We further validate our results with self-consistent mean-field calculations in a grand canonical ensemble [47,60].

Excitations. The low-energy excitations provide important information about a given state of the system, as they define its dynamical response to external forces and drive transitions between different macroscopic phases. Here, we study the excitations of the AFM phase, which have no counterpart, neither in single-component BH models nor in bulk spinor Bose gases.

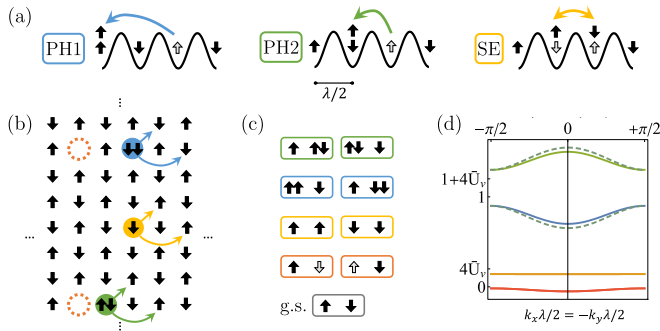


FIG. 4. Particle-hole (PH1, PH2) and spin-exchange (SE) excitations. (a) Schematic representation of the excitations in the zero-tunneling limit. (b) A finite tunneling rate enables the delocalization of the two components (quasiparticles) of each excitation [color coding as in (a)]. (c) Sketch of all possible excitation quasiparticles and (d) their band structure for $U_v/U = t/U = 0.05$. The dashed green and blue lines denote the bands when mixing of the particlelike components is included in the effective Hamiltonian. The gray box in (c) shows the doublet unit cell when no excitation quasiparticle is present, i.e., the ground state (g.s.).

We consider vanishing scalar interactions, $U_s = 0$. In the $zt/U \rightarrow 0$ limit, the AFM hosts three different low-energy excitations [Fig. 4(a)]. The two particle-hole branches PH1 and PH2 correspond to a spin transfer to lattice sites with same and opposite parity, respectively. They yield energy gaps $\Delta E_{\text{PH1}}/U = 1$ and $\Delta E_{\text{PH2}}/U = 1 + 4U_v/U$ above the ground state. The third excitation is a pairwise spin exchange (SE) involving two atoms with different spin. Its energy gap $\Delta E_{\text{SE}}/U = 8U_v/U$ can be arbitrarily tuned with respect to the PH1 and PH2 gaps by adjusting U_v .

For a finite zt/U , the two components of each excitation (particle and hole for PH1 or PH2; two exchanged spins for SE) delocalize in the lattice [Fig. 4(b)]. The effective excitation Hamiltonian

$$H_{\text{eff}} = \sum_{\mathbf{n}', \mathbf{n}} \sum_{\beta} h_{\mathbf{n}\mathbf{n}'}^{\beta} (\hat{b}_{\mathbf{n}'}^{\beta})^{\dagger} \hat{b}_{\mathbf{n}}^{\beta} + \text{H.c.} \quad (9)$$

describes quasiparticles β [Fig. 4(c)], defined on doublets of adjacent spin sites n , with creation operators $\hat{b}_{\mathbf{n}}^{\beta}$. The quasiparticles hop on a square superlattice $n_1 \mathbf{a}_1 + n_2 \mathbf{a}_2$ with $n_i \in \mathbb{Z}$, $\mathbf{n} \equiv (n_1, n_2)$, and lattice vectors $\mathbf{a}_1 = (\mathbf{e}_x + \mathbf{e}_z)\lambda/2$ and $\mathbf{a}_2 = (\mathbf{e}_x - \mathbf{e}_z)\lambda/2$. A change in the ground state configuration $|\downarrow, \uparrow\rangle$ of a doublet corresponds to the creation of a quasiparticle at that position. The coefficients $h_{\mathbf{n}\mathbf{n}'}^{\beta}$ characterize the effective tunneling strengths ($\mathbf{n}' \neq \mathbf{n}$) and energies ($\mathbf{n}' = \mathbf{n}$) of the quasiparticles. They are obtained via first-order perturbation theory, by including up to fourth-order tunneling processes and doubly occupied states [47]. We find that the SE excitation energy obtains a second-order leading correction due to tunneling. In the long-wavelength limit it reads:

$$\frac{\Delta E_{\text{SE}}}{U} = 8 \left(\frac{U_v}{U} - \frac{2(3 - 4U_v/U)}{(1 - 4U_v/U)(1 + 4U_v/U)} \left(\frac{t}{U} \right)^2 \right). \quad (10)$$

In the resulting band structure [Fig. 4(d)], all the bands are eight times degenerate, four times due to the C_4 symmetry

invariance of the two excitation components (e.g., particle left, right, above, or below the hole), and two times due to two possible configurations of each doublet. The bandwidth of the spin-exchange branches is $\sim t^4$, resulting in an extremely flat band in the considered regime, $t \approx U_v \ll U$. The bandwidths of the two particlelike branches are $\sim t^2$, and increase if weak mixing through a first-order tunneling process is included [47]. Additional mixing and level crossing of the four branches would arise through fourth-order interaction terms in Eq. (9), which we expect to become pronounced as tunneling is increased and the transition to the AF-SS is approached.

Conclusion and outlook. We considered an experimentally viable two-component spin BH model, featuring tunable vectorial and scalar cavity-assisted global-range interactions. Its phase diagram at unity filling exhibits both density- and spin-modulated superfluid and insulating phases. We discovered that the insulating spin-modulated phase with global antiferromagnetic order is stabilized for arbitrarily small vectorial interactions, due to their cooperation with repulsive contact interactions. These phases could be readily detected in existing experiments by a combination of cavity field heterodyne detection and time of flight imaging [21,23] as density and spin-modulated phases couple to orthogonal quadratures of the cavity field. While dominating intraspin contact interactions always lead to spatially homogeneous phases, larger interspin interactions give rise to phase separation in the SF and CDW phases. In addition, global-range interactions lead to unstable regions of density- and spin-modulated supersolid phases. The low-lying excitations above the AFM feature an additional spin-exchange branch, which delocalizes at finite tunneling strengths. A perturbative approach shows that its energy gap can be independently tuned via the vectorial interactions. The inclusion of quasiparticle interactions in the effective theory could enable an inspection of the mechanisms by which the interplay between different excitations drives the phase transitions.

As a direct extension, it would be interesting to study the first-order phase transition between the density- and the spin-modulated insulating phases. Two key questions there are the lifetime and decay of metastable states [22], and the spread of correlated quasiparticle excitations which might exhibit an unbounded velocity due to global-range interactions [61,62]. Moreover, regions of phase coexistence could arise when taking into account the harmonic trapping potential [11,16]. In the absence of lattices, cavity dissipation couples density- and spin-modulated states, leading to chiral instabilities and limit cycles [63–65]. The lattice system offers an experimentally tunable access to the boundary between density- and spin-modulated insulating phases, and can help clarify the fate of these instabilities in the Hubbard regime. This could provide a deeper understanding of the non-Hermitian dynamics in strongly-correlated quantum systems. Finally, the inclusion of spin-changing processes, such as local spin-spin interactions [52] or global cavity-mediated Raman processes [25,66], would give rise to another competing scale in the system and could induce novel phases like spin-density waves or chiral states [34,37].

Acknowledgments. We are grateful to Manuele Landini, Francesco Ferri, Fabian Finger, and Tobias Donner for

inspiring discussions. R.R.-M. and T.E. acknowledge funding from the Swiss National Science Foundation: Project No. 200020_212168 and No. 20QT-1_205584 and NCCR QSIT (Grant No. 51NF40-185902), and from EU Horizon2020: ERC advanced grant TransQ (Project No. 742579).

R.R.M., S.D.H., T.E., and T.D. conceived the project. L.C. derived the theoretical model and performed the

grand-canonical and perturbative calculations of the phase diagrams. N.D. performed the canonical calculations of the phase diagrams. T.D. performed the perturbative calculations related to the excitations. L.C., R.R.M., N.D., and T.D. wrote the manuscript. R.R.M., N.D., and T.D. supervised the project. All authors contributed to the discussion and interpretation of the results.

-
- [1] D. Jaksch, C. Bruder, J. I. Cirac, C. W. Gardiner, and P. Zoller, Cold Bosonic Atoms in Optical Lattices, *Phys. Rev. Lett.* **81**, 3108 (1998).
- [2] M. Greiner, O. Mandel, T. Esslinger, T. W. Hänsch, and I. Bloch, Quantum phase transition from a superfluid to a Mott insulator in a gas of ultracold atoms, *Nature (London)* **415**, 39 (2002).
- [3] C. Gross and I. Bloch, Quantum simulations with ultracold atoms in optical lattices, *Science* **357**, 995 (2017).
- [4] F. Schäfer, T. Fukuhara, S. Sugawa, Y. Takasu, and Y. Takahashi, Tools for quantum simulation with ultracold atoms in optical lattices, *Nat. Rev. Phys.* **2**, 411 (2020).
- [5] V. Vuletić, A. J. Kerman, C. Chin, and S. Chu, Observation of Low-Field Feshbach Resonances in Collisions of Cesium Atoms, *Phys. Rev. Lett.* **82**, 1406 (1999).
- [6] S. A. Moses, J. P. Covey, M. T. Miecnikowski, D. S. Jin, and J. Ye, New frontiers for quantum gases of polar molecules, *Nat. Phys.* **13**, 13 (2017).
- [7] T. Lahaye, C. Menotti, L. Santos, M. Lewenstein, and T. Pfau, The physics of dipolar bosonic quantum gases, *Rep. Prog. Phys.* **72**, 126401 (2009).
- [8] A. Browaeys, D. Barredo, and T. Lahaye, Experimental investigations of dipole–dipole interactions between a few Rydberg atoms, *J. Phys. B: At. Mol. Opt. Phys.* **49**, 152001 (2016).
- [9] H. Ritsch, P. Domokos, F. Brennecke, and T. Esslinger, Cold atoms in cavity-generated dynamical optical potentials, *Rev. Mod. Phys.* **85**, 553 (2013).
- [10] F. Mivehvar, F. Piazza, T. Donner, and H. Ritsch, Cavity QED with quantum gases: new paradigms in many-body physics, *Adv. Phys.* **70**, 1 (2021).
- [11] Y. Li, L. He, and W. Hofstetter, Lattice-supersolid phase of strongly correlated bosons in an optical cavity, *Phys. Rev. A* **87**, 051604(R) (2013).
- [12] M. R. Bakhtiari, A. Hemmerich, H. Ritsch, and M. Thorwart, Nonequilibrium Phase Transition of Interacting Bosons in an Intra-Cavity Optical Lattice, *Phys. Rev. Lett.* **114**, 123601 (2015).
- [13] S. F. Caballero-Benitez and I. B. Mekhov, Quantum Optical Lattices for Emergent Many-Body Phases of Ultracold Atoms, *Phys. Rev. Lett.* **115**, 243604 (2015).
- [14] N. Dogra, F. Brennecke, S. D. Huber, and T. Donner, Phase transitions in a Bose-Hubbard model with cavity-mediated global-range interactions, *Phys. Rev. A* **94**, 023632 (2016).
- [15] Y. Chen, Z. Yu, and H. Zhai, Quantum phase transitions of the Bose-Hubbard model inside a cavity, *Phys. Rev. A* **93**, 041601(R) (2016).
- [16] B. Sundar and E. J. Mueller, Lattice bosons with infinite-range checkerboard interactions, *Phys. Rev. A* **94**, 033631 (2016).
- [17] T. Flottat, L. de Forges de Parny, F. Hébert, V. G. Rousseau, and G. G. Batrouni, Phase diagram of bosons in a two-dimensional optical lattice with infinite-range cavity-mediated interactions, *Phys. Rev. B* **95**, 144501 (2017).
- [18] R. Liao, H.-J. Chen, D.-C. Zheng, and Z.-G. Huang, Theoretical exploration of competing phases of lattice Bose gases in a cavity, *Phys. Rev. A* **97**, 013624 (2018).
- [19] H.-J. Chen, Y.-Q. Yu, D.-C. Zheng, and R. Liao, Extended bose-hubbard model with cavity-mediated infinite-range interactions at finite temperatures, *Sci. Rep.* **10**, 9076 (2020).
- [20] J. Klinder, H. Keßler, M. R. Bakhtiari, M. Thorwart, and A. Hemmerich, Observation of a Superradiant Mott Insulator in the Dicke-Hubbard Model, *Phys. Rev. Lett.* **115**, 230403 (2015).
- [21] R. Landig, L. Hruby, N. Dogra, M. Landini, R. Mottl, T. Donner, and T. Esslinger, Quantum phases from competing short- and long-range interactions in an optical lattice, *Nature (London)* **532**, 476 (2016).
- [22] L. Hruby, N. Dogra, M. Landini, T. Donner, and T. Esslinger, Metastability and avalanche dynamics in strongly correlated gases with long-range interactions, *Proc. Natl. Acad. Sci.* **115**, 3279 (2018).
- [23] M. Landini, N. Dogra, K. Kroeger, L. Hruby, T. Donner, and T. Esslinger, Formation of a Spin Texture in a Quantum Gas Coupled to a Cavity, *Phys. Rev. Lett.* **120**, 223602 (2018).
- [24] R. M. Kroeze, Y. Guo, V. D. Vaidya, J. Keeling, and B. L. Lev, Spinor Self-Ordering of a Quantum Gas in a Cavity, *Phys. Rev. Lett.* **121**, 163601 (2018).
- [25] F. Ferri, R. Rosa-Medina, F. Finger, N. Dogra, M. Soriente, O. Zilberberg, T. Donner, and T. Esslinger, Emerging Dissipative Phases in a Superradiant Quantum Gas with Tunable Decay, *Phys. Rev. X* **11**, 041046 (2021).
- [26] J. Simon, H. Tanji, S. Ghosh, and V. Vuletić, Single-photon bus connecting spin-wave quantum memories, *Nat. Phys.* **3**, 765 (2007).
- [27] P. Strack and S. Sachdev, Dicke Quantum Spin Glass of Atoms and Photons, *Phys. Rev. Lett.* **107**, 277202 (2011).
- [28] S. Gopalakrishnan, B. L. Lev, and P. M. Goldbart, Frustration and Glassiness in Spin Models with Cavity-Mediated Interactions, *Phys. Rev. Lett.* **107**, 277201 (2011).
- [29] M. Buchhold, P. Strack, S. Sachdev, and S. Diehl, Dicke-model quantum spin and photon glass in optical cavities: Nonequilibrium theory and experimental signatures, *Phys. Rev. A* **87**, 063622 (2013).
- [30] Z. Zhiqiang, C. H. Lee, R. Kumar, K. J. Arnold, S. J. Masson, A. S. Parkins, and M. D. Barrett, Nonequilibrium phase transition in a spin-1 Dicke model, *Optica* **4**, 424 (2017).
- [31] F. Mivehvar, F. Piazza, and H. Ritsch, Disorder-Driven Density and Spin Self-Ordering of a Bose-Einstein Condensate in a Cavity, *Phys. Rev. Lett.* **119**, 063602 (2017).
- [32] R. J. Lewis-Swan, M. A. Norcia, J. R. K. Cline, J. K. Thompson, and A. M. Rey, Robust Spin Squeezing via Photon-Mediated

- Interactions on an Optical Clock Transition, *Phys. Rev. Lett.* **121**, 070403 (2018).
- [33] E. J. Davis, G. Bentsen, L. Homeier, T. Li, and M. H. Schleier-Smith, Photon-Mediated Spin-Exchange Dynamics of Spin-1 Atoms, *Phys. Rev. Lett.* **122**, 010405 (2019).
- [34] F. Mivehvar, H. Ritsch, and F. Piazza, Cavity-Quantum-Electrodynamical Toolbox for Quantum Magnetism, *Phys. Rev. Lett.* **122**, 113603 (2019).
- [35] J. A. Muniz, D. Barberena, R. J. Lewis-Swan, D. J. Young, J. R. K. Cline, A. M. Rey, and J. K. Thompson, Exploring dynamical phase transitions with cold atoms in an optical cavity, *Nature (London)* **580**, 602 (2020).
- [36] K. C. Stitely, A. Giraldo, B. Krauskopf, and S. Parkins, Non-linear semiclassical dynamics of the unbalanced, open Dicke model, *Phys. Rev. Res.* **2**, 033131 (2020).
- [37] X. Guan, J. Fan, X. Zhou, G. Chen, and S. Jia, Two-component lattice bosons with cavity-mediated long-range interaction, *Phys. Rev. A* **100**, 013617 (2019).
- [38] K. Lozano-Méndez, A. H. Cásares, and S. F. Caballero-Benítez, Spin Entanglement and Magnetic Competition via Long-Range Interactions in Spinor Quantum Optical Lattices, *Phys. Rev. Lett.* **128**, 080601 (2022).
- [39] J. Fan, X. Zhou, W. Zheng, W. Yi, G. Chen, and S. Jia, Magnetic order in a Fermi gas induced by cavity-field fluctuations, *Phys. Rev. A* **98**, 043613 (2018).
- [40] A. Camacho-Guardian, R. Paredes, and S. F. Caballero-Benítez, Quantum simulation of competing orders with fermions in quantum optical lattices, *Phys. Rev. A* **96**, 051602(R) (2017).
- [41] A. B. Kuklov and B. V. Svistunov, Counterflow Superfluidity of Two-Species Ultracold Atoms in a Commensurate Optical Lattice, *Phys. Rev. Lett.* **90**, 100401 (2003).
- [42] E. Altman, W. Hofstetter, E. Demler, and M. D. Lukin, Phase diagram of two-component bosons on an optical lattice, *New J. Phys.* **5**, 113 (2003).
- [43] F. Lingua, M. Guglielmino, V. Penna, and B. Capogrosso Sansone, Demixing effects in mixtures of two bosonic species, *Phys. Rev. A* **92**, 053610 (2015).
- [44] R. Bai, D. Gaur, H. Sable, S. Bandyopadhyay, K. Suthar, and D. Angom, Segregated quantum phases of dipolar bosonic mixtures in two-dimensional optical lattices, *Phys. Rev. A* **102**, 043309 (2020).
- [45] D.-C. Zhang, S.-P. Feng, and S.-J. Yang, Quantum phases of two-component bosons in the extended Bose-Hubbard model, *Phys. Lett. A* **427**, 127912 (2022).
- [46] G. G. Batrouni and R. T. Scalettar, Phase Separation in Super-solids, *Phys. Rev. Lett.* **84**, 1599 (2000).
- [47] See Supplemental Material at <http://link.aps.org/supplemental/10.1103/PhysRevResearch.5.L032003> for the derivation of the model, the details and comparison of the methods employed to obtain the phase diagrams, and the derivation of the effective Hamiltonian for excitations.
- [48] F. L. Kien, P. Schneeweiss, A. Rauschenbeutel, F. Le Kien, P. Schneeweiss, and A. Rauschenbeutel, Dynamical polarizability of atoms in arbitrary light fields: general theory and application to cesium, *Eur. Phys. J. D* **67**, 92 (2013).
- [49] C. Cohen-Tannoudji, J. Dupont-Roc, and G. Grynberg, *Atom-Photon Interactions: Basic Processes and Applications* (VCH PUBN, 1998).
- [50] W. Zwerger, Mott-Hubbard transition of cold atoms in optical lattices, *J. Opt. B: Quantum Semiclassical Opt.* **5**, S9 (2003).
- [51] M. P. A. Fisher, P. B. Weichman, G. Grinstein, and D. S. Fisher, Boson localization and the superfluid-insulator transition, *Phys. Rev. B* **40**, 546 (1989).
- [52] D. M. Stamper-Kurn and M. Ueda, Spinor Bose gases: Symmetries, magnetism, and quantum dynamics, *Rev. Mod. Phys.* **85**, 1191 (2013).
- [53] D. S. Rokhsar and B. G. Kotliar, Gutzwiller projection for bosons, *Phys. Rev. B* **44**, 10328 (1991).
- [54] E. Altman and A. Auerbach, Oscillating Superfluidity of Bosons in Optical Lattices, *Phys. Rev. Lett.* **89**, 250404 (2002).
- [55] S. D. Huber, E. Altman, H. P. Büchler, and G. Blatter, Dynamical properties of ultracold bosons in an optical lattice, *Phys. Rev. B* **75**, 085106 (2007).
- [56] D. van Oosten, P. van der Straten, and H. T. C. Stoof, Quantum phases in an optical lattice, *Phys. Rev. A* **63**, 053601 (2001).
- [57] P. M. Chaikin and T. C. Lubensky, Principles of condensed matter physics, in *Principles of Condensed Matter Physics* (Cambridge University Press, 1995), pp. 144–212.
- [58] G.-H. Chen and Y.-S. Wu, Quantum phase transition in a multicomponent Bose-Einstein condensate in optical lattices, *Phys. Rev. A* **67**, 013606 (2003).
- [59] J. Zhao, S. Hu, J. Chang, P. Zhang, and X. Wang, Ferromagnetism in a two-component Bose-Hubbard model with synthetic spin-orbit coupling, *Phys. Rev. A* **89**, 043611 (2014).
- [60] A. Dhar, M. Singh, R. V. Pai, and B. P. Das, Mean-field analysis of quantum phase transitions in a periodic optical superlattice, *Phys. Rev. A* **84**, 033631 (2011).
- [61] M. Cheneau, P. Barmettler, D. Poletti, M. Endres, P. Schauß, T. Fukuhara, C. Gross, I. Bloch, C. Kollath, and S. Kuhr, Light-cone-like spreading of correlations in a quantum many-body system, *Nature (London)* **481**, 484 (2012).
- [62] P. Hauke and L. Tagliacozzo, Spread of Correlations in Long-Range Interacting Quantum Systems, *Phys. Rev. Lett.* **111**, 207202 (2013).
- [63] N. Dogra, M. Landini, K. Kroeger, L. Hruby, T. Donner, and T. Esslinger, Dissipation-induced structural instability and chiral dynamics in a quantum gas, *Science* **366**, 1496 (2019).
- [64] E. I. Rodríguez Chiacchio and A. Nunnenkamp, Dissipation-Induced Instabilities of a Spinor Bose-Einstein Condensate Inside an Optical Cavity, *Phys. Rev. Lett.* **122**, 193605 (2019).
- [65] B. Buča and D. Jaksch, Dissipation Induced Nonstationarity in a Quantum Gas, *Phys. Rev. Lett.* **123**, 260401 (2019).
- [66] R. Rosa-Medina, F. Ferri, F. Finger, N. Dogra, K. Kroeger, R. Lin, R. Chitra, T. Donner, and T. Esslinger, Observing Dynamical Currents in a Non-Hermitian Momentum Lattice, *Phys. Rev. Lett.* **128**, 143602 (2022).